

BABCOCK-LEIGHTON SOLAR DYNAMO: THE ROLE OF DOWNWARD PUMPING AND THE EQUATORWARD PROPAGATION OF ACTIVITY

BIDYA BINAY KARAK^{1,2} AND ROBERT CAMERON¹

¹Max-Planck-Institut für Sonnensystemforschung, Justus-von-Liebig-Weg 3, D-37077 Göttingen, Germany

¹High Altitude Observatory, National Center for Atmospheric Research, 3080 Center Green Dr., Boulder, CO 80301, USA

Draft version October 13, 2018

ABSTRACT

The key elements of the Babcock-Leighton dynamos are the generation of poloidal field through decay and dispersal of tilted bipolar active regions and the generation of toroidal field through the observed differential rotation. These models are traditionally known as flux transport dynamo models as the equatorward propagations of the butterfly wings in these models are produced due to an equatorward flow at the bottom of the convection zone. Here we investigate the role of downward magnetic pumping near the surface using a kinematic Babcock-Leighton model. We find that the pumping causes the poloidal field to become predominately radial in the near-surface shear layer, which allows the negative radial shear to effectively act on the radial field to produce a toroidal field. We observe a clear equatorward migration of the toroidal field at low latitudes as a consequence of the dynamo wave even when there is no meridional flow in the deep convection zone. Both the dynamo wave and the flux transport type solutions are thus able to reproduce some of the observed features of the solar cycle, including the 11-year periodicity. The main difference between the two types of solutions is the strength of the Babcock-Leighton source required to produce the dynamo action. A second consequence of the magnetic pumping is that it suppresses the diffusion of fields through the surface, which helps to allow an 11-year cycle at (moderately) larger values of magnetic diffusivity than have previously been used.

Subject headings:

1. INTRODUCTION

In most models of the solar dynamo, there are two key processes: the generation of toroidal magnetic field by winding up of poloidal field by differential rotation (Ω effect) and the generation of poloidal magnetic field by flows associated with small-scale motions, influenced by the Coriolis force, acting on the toroidal field (α effect); see Charbonneau (2014) for a review. Recently we have strong observational supports that the dynamo is of the Babcock-Leighton type, where the poloidal field is produced from the decay and dispersal of tilted active regions near the surface (e.g., Dasi-Espuig et al. 2010; Kitchatinov & Olemskoy 2011; Cameron & Schüssler 2015). Although these papers constrain the nature of dynamo mechanism operating in the Sun, they do not address the questions of why the butterfly wings (the latitudes at which sunspots emerge) drift equatorward, and why the dynamo period is about 11 years.

We are not the first to address these questions. For the equatorward migration, two main possible mechanisms are available in the literature. The first mechanism to appear was that of Parker (1955), and it corresponds to a dynamo wave, where the propagation is on surfaces of constant rotation (Yoshimura 1975). Hence, the radial differential rotation gives rise to a latitudinal migration. This is known as the Parker-Yoshimura sign rule. According to this rule, the direction of propagation (poleward or equatorward) depends on the sign of the α effect (the sense of the helical motion), and the sign of the radial shear. To have equatorward propagation in the Sun where α is positive in the northern hemisphere, differential rotation must increase inwards (Yoshimura 1975).

From 1955 to the mid-1980s, this dynamo-wave model was widely accepted. However, a decline in the popularity of this model followed from a combination of the sugges-

tion by Parker (1975) that, in order to maintain organized toroidal flux over many years, the field must be stored at the base of the solar convection zone (SCZ), and the discovery using helioseismology that the differential rotation in the low-latitude tachocline decreases inwards, which would lead to poleward propagation of the butterfly wings – contrary to what is observed. One possibility to obtain the equatorward migration with the field still being at the base of CZ, where the radial shear is positive, is if the α is negative (in the northern hemisphere) there, as is observed in some three-dimensional convection simulations (e.g., Brandenburg et al. 1990; Augustson et al. 2015; Warnecke et al. 2016),

The question of how to obtain the equatorward migration of the activity belt outside the dynamo-wave framework led to the identification of a second possible mechanism, the flux transport dynamo (FTD) model (Wang et al. 1991; Choudhuri et al. 1995; Durney 1995). In this model, it is assumed that an equatorward velocity near the base of the CZ overpowers the poleward propagating dynamo wave and leads to a net equatorward migration in the toroidal flux that produces sunspot eruptions.

However, more recently three-dimensional convective dynamo simulations have shown, contrary to the suggestion of Parker (1975), that substantial organized toroidal magnetic field can be stored in the CZ for periods of years (Brown et al. 2010). Furthermore, storage in the tachocline has been shown to be problematic (Weber & Fan 2015), and concerns have been raised about the ability to extract energy from the radial shear in the tachocline (Vasil & Brummell 2009; Spruit 2011). This has led to an increasing support for the dynamo wave explanation for the equatorward migration with the near-surface shear layer (NSSL), where the differential rotation increases inwards (e.g., Brandenburg 2005; Käpylä et al. 2006; Brandenburg 2009; Pipin & Kosovichev 2011).

Returning to the other question—why the dynamo period

is 11 years—sheds light on the two possibilities. In a simple oscillatory $\alpha\Omega$ dynamo, the cycle period is inversely related to the turbulent diffusivity η as well as dependence on α and shear. This leads to a short cycle period of 2–3 years (using a value of $\eta \sim 10^{12-13} \text{ cm}^2 \text{ s}^{-1}$ —an estimation based on the mixing length theory; Köhler 1973; Karak & Choudhuri 2012). A similar difficulty also appears in the Babcock–Leighton type FTD models. Therefore FTD models have used much lower values of η than the mixing length estimates, so that the cycle period is predominately determined by the speed of the meridional flow near the bottom (Dikpati & Charbonneau 1999; Karak 2010).

One physical justification for the use of this weaker value of η in dynamo models was that the magnetic quenching could reduce η significantly from its mixing length value (Rüdiger et al. 1994; Guerrero et al. 2009; Muñoz-Jaramillo et al. 2011). Indeed, there is evidence of magnetic quenching in various numerical simulations, although most of the simulations at present are performed in parameters regimes far from the SCZ (e.g., Käpylä & Brandenburg 2009; Karak et al. 2014c). The latter authors, however, found substantial quenching only when the mean magnetic field is substantially greater than the equipartition field strength (based on the energy in the convective motions). In particular, a reduction of η by two orders of magnitude (from $10^{13} \text{ cm}^2 \text{ s}^{-1}$ to $10^{11} \text{ cm}^2 \text{ s}^{-1}$) requires the mean magnetic field to be larger than the equipartition value by more than two orders of magnitude (also see Simard et al. 2016, who support this result). Such field strengths are not plausible. Another possibility for weaker diffusion is that changes in the mean flows (e.g., the inflow observed around active regions) could play a role (Cameron & Schüssler 2016). In any case, exploring the range of values of η for which the Babcock–Leighton dynamos have equatorial propagation and the 11-year period is a useful exercise.

In this article, we construct a Babcock–Leighton dynamo model and explore how the radial pumping affects equatorward migration and the cycle period in both FTD and dynamo wave frameworks. For both models, differential rotation is an important ingredient for which we consider two different profiles. One closely corresponds to the available helioseismic data, while the other is an analytic approximation that includes the observed NSSL but neglects the radial variation in most of the CZ—from top of the tachocline to the bottom of the NSSL. The motivation for the latter profile is that it gives a maximal toroidal flux generated from magnetic flux threading the surface by the radial shear because in helioseismic profile, the radial shear has the opposite sign above and below the bottom of the NSSL. We show that for both choices of differential rotation the NSSL where the rotation rate increases inward plays an important role in producing the equatorward migration of sunspots in addition to the migration caused by the equatorward meridional flow near the bottom of the CZ. We demonstrate that a radially downward magnetic pumping makes the magnetic field more radial in the NSSL, which allows the (negative) radial shear to stretch the radial field to generate a toroidal field. This helps to produce an equatorward migration of toroidal field where the (Babcock–Leighton) α is non-zero.

Moreover, the magnetic pumping inhibits the diffusion of toroidal field through the photosphere that helps to excite dynamo with a correct period at a considerably higher value of η than it was possible in earlier. This role of the pumping

is complementary to that studied by Cameron et al. (2012) who further demonstrated that a downward pumping is crucial to match the results of FTDs with the surface flux transport model and observations.

2. MODEL

In our model, we study the axisymmetric large-scale magnetic field in the kinematic regime. Therefore the magnetic field can be written as

$$\mathbf{B} = \mathbf{B}_p + \mathbf{B}_\phi = \nabla \times [A(r, \theta, t)\hat{\phi}] + B(r, \theta, t)\hat{\phi}, \quad (1)$$

where $\mathbf{B}_p = \nabla \times [A\hat{\phi}]$ is the poloidal component of the magnetic field and B is the toroidal component. Similarly the velocity field can be written as

$$\mathbf{v} = \mathbf{v}_p + \mathbf{v}_\phi = v_r(r, \theta)\hat{r} + v_\theta(r, \theta)\hat{\theta} + r \sin \theta \Omega(r, \theta)\hat{\phi}, \quad (2)$$

where v_r and v_θ correspond to the meridional circulation and Ω is the angular frequency. Then, the evolution equations of A and B in the flux transport dynamo model become followings.

$$\frac{\partial A}{\partial t} + \frac{1}{s}(\mathbf{v}_p \cdot \nabla)(sA) = \eta \left(\nabla^2 - \frac{1}{s^2} \right) A + S(r, \theta; B), \quad (3)$$

$$\begin{aligned} \frac{\partial B}{\partial t} + \frac{1}{r} \left[\frac{\partial}{\partial r}(rv_r B) + \frac{\partial}{\partial \theta}(v_\theta B) \right] &= \eta \left(\nabla^2 - \frac{1}{s^2} \right) B \\ &+ s(\mathbf{B}_p \cdot \nabla)\Omega + \frac{1}{r} \frac{d\eta}{dr} \frac{\partial(rB)}{\partial r}, \end{aligned} \quad (4)$$

where $s = r \sin \theta$.

For the meridional circulation we define a stream function ψ such that $\rho \mathbf{v}_p = \nabla \times [\psi(r, \theta)\mathbf{e}_\phi]$, where $\rho = C \left(\frac{R}{r} - 0.95 \right)^{3/2}$, and

$$\begin{aligned} \psi r \sin \theta &= \psi_0(r - R_p) \sin \left[\frac{\pi(r - R_p)}{(R - R_p)} \right] \{1 - e^{-\beta_1 \theta^\epsilon}\} \\ &\times \{1 - e^{\beta_2(\theta - \pi/2)}\} e^{-((r - r_0)/\Gamma)^2} \end{aligned} \quad (5)$$

with $\beta_1 = 1.5$, $\beta_2 = 1.3$, $\epsilon = 2.0000001$, $r_0 = 0.45R/3.5$, $\Gamma = 3.47 \times 10^8 \text{ m}$, and $R_p = 0.7R$. The value of ψ_0/C is chosen in such a way that the amplitude of the meridional circulation at mid-latitudes v_0 becomes 20 m s^{-1} . Our profile is very similar to many previous publications, particularly Hazra et al. (2014) (see their Eqs. 6–8) except here we assume that the meridional flow smoothly goes to zero at $0.7R$. The resulting variation is shown in Figure 1. We note that our results are not very sensitive to the detailed flow structure in the CZ as long as we have a reasonable amount of poleward flow near the surface. Towards the end of this article (§4.3), we shall show that we get the correct magnetic cycle even with a shallow meridional circulation residing only in the upper $0.8R$.

In addition to the large-scale meridional circulation, we add a magnetic pumping, the γ effect in our model. This γ appears as an advective term in the mean-field induction equation. Unlike the large-scale circulation, γ is not divergenceless. Theoretical analysis and local magneto-convection simulations predict a downward magnetic pumping in the SCZ (Drobyshevski & Yuferev 1974; Krause & Rädler 1980; Petrovay & Szakaly 1993; Tobias et al. 1998; Käpylä et al.

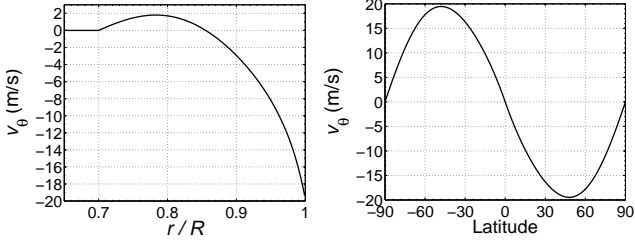


Figure 1. Radial and latitudinal dependences of the latitudinal component of the meridional flow v_θ at 45° latitude (left panel) and at the surface (right), respectively.

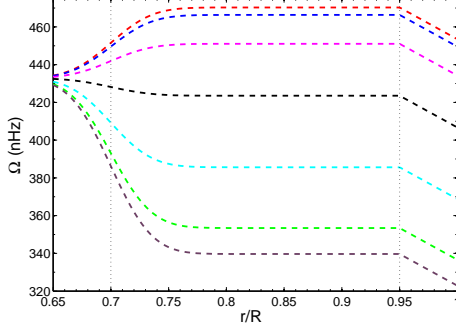


Figure 2. Radial variations of the angular frequencies at 0 (red), 15, 30 (pink), 45, 60, 75 (green) and 90 degree latitudes based on Equation (7).

2009; Karak et al. 2014c). The recent rapidly rotating convection simulations in stellar CZs (e.g., Augustson et al. 2015; Warnecke et al. 2016) also find magnetic pumping, although in some cases, it is radially outward at some latitudes. These simulations, however, may not represent the actual picture because they do not capture the realistic physics of the solar surface convection and even they do not extend to the top surface, where a strong pumping can be inferred from the success of the surface flux transport model (Cameron et al. 2012). (See also Guerrero & de Gouveia Dal Pino 2008; Karak & Nandy 2012; Jiang et al. 2013, who demonstrated the importance of downward pumping in simulating the solar cycle.) Hence, in our study we assume that it is downward and only significant in the top 10% of the Sun. This assumption is supported by a number of facts that the upper layer of the Sun is highly unstable to convection while the deeper layer is only weakly unstable (Spruit 1997), convection is very weak below the surface layer (Hanasoge et al. 2012), and a huge density stratification near the surface.

Therefore in Equation (2), we replace v_r by $v_r + \gamma_r$ where

$$\gamma_r(r) = -\frac{\gamma_{r0}}{2} \left[1 + \operatorname{erf} \left(\frac{r - 0.9R}{0.02R} \right) \right]. \quad (6)$$

Due to the lack of knowledge of the exact latitudinal variation of γ_r , we take it to be only a function of radius. This is indeed a good choice based on the high Rossby number of the surface convection. The value of γ_{r0} is not directly constrained by observations and we take it as a free parameter.

For angular frequency we take two different profiles. First, we choose a simplified analytical form given by

$$\Omega(r, \theta) = \Omega_{\text{RZ}} + \frac{\Omega_{\text{CZ}} - \Omega_{\text{RZ}}}{2} \left[1 + \operatorname{erf} \left(\frac{r - 0.7R}{0.04R} \right) \right]. \quad (7)$$

Here $\Omega_{\text{RZ}}/2\pi = 432.8$ nHz, and $\Omega_{\text{CZ}}/2\pi = \Omega_1$ for $r < 0.95R$, while $\Omega_{\text{CZ}}/2\pi = \Omega_1 - a_s(r - 0.95R)/0.05R$

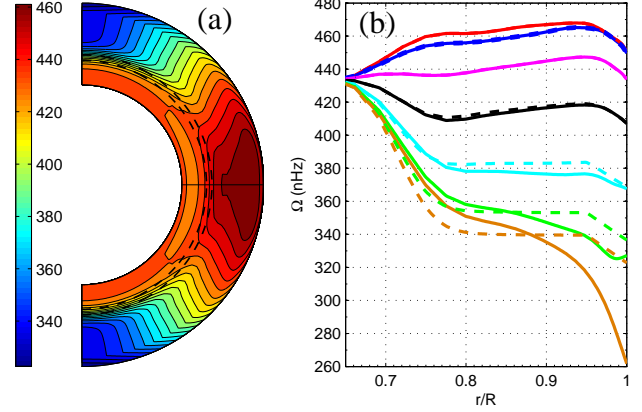


Figure 3. (a): Rotational frequencies of Sun (in nHz) as obtained from helioseismic data combined with the analytical profile for higher latitudes. (b): comparison of helioseismic data (solid lines) and our composite (dashed) profile at 0 (red), 15, 30 (pink), 45, 60, 75 (green) and 90 degree latitudes.

for $r \geq 0.95R$, where $\Omega_1 = 470.308 - 62.79 \cos^2 \theta - 67.87 \cos^4 \theta$ nHz and $a_s = 16.808$ nHz. This type of simple profile, except the near-surface shear layer, is used in many previous flux transport dynamo models (except, Dikpati et al. 2002; Guerrero & de Gouveia Dal Pino 2008). The radial variation of this Ω at different latitudes is shown in Figure 2. Later in §4 we shall use the observed rotation profile from helioseismology, kindly provided by J. Schou. However, these measurements are not reliable in high latitudes. Therefore we construct a composite profile using the above analytical profile for high latitudes where the observed data is less reliable. The composite Ω to be used in our dynamo model is shown in Figure 3.

For the turbulent magnetic diffusivity, we choose the following radial dependent profile motivated by previous models (e.g., Dikpati et al. 2002):

$$\eta(r) = \eta_{\text{RZ}} + \frac{\eta_{\text{CZ}} - \eta_{\text{RZ}}}{2} \left[1 + \operatorname{erf} \left(\frac{r - 0.69R}{0.01R} \right) \right] + \frac{\eta_{\text{surf}} - \eta_{\text{CZ}} - \eta_{\text{RZ}}}{2} \left[1 + \operatorname{erf} \left(\frac{r - 0.95R}{0.01R} \right) \right], \quad (8)$$

where $\eta_{\text{RZ}} = 2.2 \times 10^8 \text{ cm}^2 \text{ s}^{-1}$, $\eta_{\text{surf}} = 3 \times 10^{12} \text{ cm}^2 \text{ s}^{-1}$. While the diffusivity near the surface is constrained by observations as well as by the surface flux transport model (e.g., Komm et al. 1995; Lemerle et al. 2015), the diffusivity in the deeper CZ is poorly known. For most of the simulations, we choose $\eta_{\text{CZ}} = 5 \times 10^{11} \text{ cm}^2 \text{ s}^{-1}$; however in some simulations we vary it up to $10 \times 10^{11} \text{ cm}^2 \text{ s}^{-1}$. The radial dependence of η is shown in Figure 4.

Finally, the source term $S(r, \theta; B)$, which captures the Babcock–Leighton mechanism for the generation of poloidal field near the solar surface from the decay of tilted bipolar active regions, has the following form:

$$S(r, \theta; B) = \alpha^{\text{BL}}(r, \theta) \overline{B}(\theta). \quad (9)$$

Here,

$$\alpha^{\text{BL}}(r, \theta) = \alpha_0 f_\alpha(\theta) \frac{1}{2} \left[1 + \operatorname{erf} \left(\frac{r - 0.95R}{0.01R} \right) \right], \quad (10)$$

where α_0 determines the strength of the Babcock–Leighton α which is set to a value for which we get a nearly stable

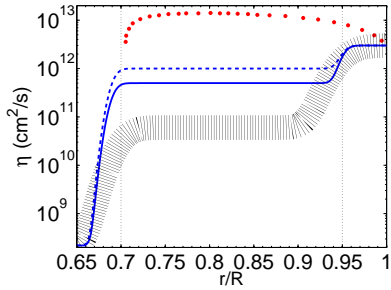


Figure 4. Radial variations of the turbulent diffusivity (solid line) and its allowed upper value (dashed line) in our model. Lower shaded region and upper red points represent typical values used in most previous FTD models and the mixing-length theory.

solution, and

$$f_{\alpha}(\theta) = \cos \theta \sin^n \theta. \quad (11)$$

The radial dependence in Equation (10) ensures that the Babcock–Leighton process only operates near the surface above $0.95R$. The latitudinal dependence of $f_{\alpha}(\theta)$ is chosen in such a way that $S(r, \theta; B)$ is negligible above $\pm 30^\circ$ latitudes where we do not observe much sunspots. This sets the value of n to 12. But in a few cases, we change it to two. We note that previous dynamo modelers also artificially suppress the production of poloidal field above 30° latitudes (e.g., Karak et al. 2014b; Muñoz-Jaramillo et al. 2011; Miesch & Teweldebirhan 2016).

In some simulations discussed below, we take $\overline{B}(\theta)$ as the mean (area normalized) toroidal field over the whole CZ: $\int_{0.7R}^R B(r, \theta) r dr / \int_{0.7R}^R r dr$. For comparison with traditional FTD simulations, in some cases, we also take $\overline{B}(\theta)$ as the radial-averaged toroidal field over the tachocline from $0.7R$ to $0.71R$. Which choice we make for $\overline{B}(\theta)$ will be given below in the description of individual numerical experiments we have performed. We note that in our α (Equation (9)), we do not include any nonlinearity to saturate the poloidal field production, which is common in any kinematic dynamo model (Karak et al. 2014a).

The computational domain of our model is $0.55R \leq r \leq R$ and $0 \leq \theta \leq \pi$. For the boundary conditions, we use $A, B = 0$ at poles and at the bottom, while $\frac{\partial}{\partial r}(rA), B = 0$ (radial field condition) at the top. Our model is formulated using the code SURYA, developed by A. R. Choudhuri and his colleagues at Indian Institute of Science (Chatterjee et al. 2004).

3. RESULTS WITH SIMPLIFIED ROTATION PROFILE

To study the evolution of magnetic fields we solve equations (3) and (4) by prescribing all ingredients described above. For the first set of numerical experiments, we used the simple analytical profile for the differential rotation as shown in Figure 2. The advantage of using this profile is that it allows us to more easily understand the dynamics of the system. It also corresponds to the solution that maximally exploits the near-surface shear layer and hence provides the limit where the dynamo wave generated toroidal flux is maximal. When the source term in Equation (3) is non-zero, we expect oscillatory dynamo solution provided the diffusive decay of the field is less than its generation.

3.1. Evolution of magnetic fields for $\alpha^{\text{BL}} = 0$

To get an insight into the behavior at high magnetic diffusivity, we begin by studying the decay of an initial poloidal field without putting any magnetic pumping. The initial field¹ is shown in panels A of Figure 5. We then follow the evolution according to equations (3) and (4) with $\alpha_0 = 0$, i.e., with no source for the poloidal field in Equation (3). The left panels of Figure 5 show three snapshots after 5, 15 and 50 years from the beginning of the simulation. We observe that most of the poloidal field diffuses away across the surface and only in about 15 years the field has decreased by an order of magnitude.

Because of the source term in the toroidal field equation, the Ω effect, the toroidal field is generated from the poloidal field and the snapshots after 5, 15 and 50 years are shown on the right panels of Figure 5. We observe that the latitudinal differential rotation produces a significant amount toroidal field in the bulk of the CZ. Therefore after 5 years we have a substantial field. However as the diffusivity is much stronger in the upper layer ($\eta_{\text{surf}} = 3 \times 10^{12} \text{ cm}^2 \text{ s}^{-1}$ for $r \geq 0.95R$), toroidal field is much weaker there as compared to the deeper layer. We also observe much weaker field near the equator at all radii because of the diffusion of opposite polarity fields from opposite hemispheres. Along with the diffusion of the toroidal field, its source, the poloidal field itself is also decaying (compare panels A-D). Consequently the toroidal field is not amplified beyond about 5 years, rather it starts to decrease in time. This can be seen in panels G and H after 15 and 50 years, respectively.

The loss of magnetic flux becomes more transparent when we monitor the net toroidal flux diffusion rates across the solar surface: $\dot{\Phi}_{\text{tor}}^S = |\eta(R) \int_0^{\pi/2} \frac{\partial}{\partial r}(rB) d\theta|$ and across the equator: $\dot{\Phi}_{\text{tor}}^E = |\int_{0.55R}^R \eta(r) (r \sin \theta)^{-1} \frac{\partial}{\partial \theta}(\sin \theta B) dr|$, for the northern hemisphere (in arbitrary unit) which are displayed in Figure 7. We note that fluxes across the lower boundary and at the pole are not significant and we do not present them here.

The knowledge we gain from above experiment is that the diffusion of fields across the solar surface is extremely important for the dynamics in the high diffusivity regime. We conjectured that a magnetic pumping in the upper layer of the CZ could inhibit the diffusion of the horizontal fields across the surface and radically change the dynamics. To test this idea, we repeated the previous numerical experiment with 35 m s^{-1} pumping operating above $0.9R$. Snapshots of poloidal and toroidal fields at 5, 15 and 50 years from this simulation are shown in Figure 6. In comparison to the initial strength (shown in Figure 5A), we observe that after 5 years the poloidal field has reduced by some extent because of the diffusion across the equator. As expected from Cameron et al. (2012), the evolution of the poloidal field is very slow after this time; compare panels B-D in Figure 6. The difference in poloidal fields between the simulations with and without pumping is due to the strongly reduced diffusion across the surface. We further notice that the poloidal field in the near-surface shear layer where the pumping is operating becomes largely radial. The poleward meridional flow advects this field to high latitudes and once this field reaches there, there is no way to escape. The poloidal field remains in high latitudes for several thousands of years, which is confirmed by continuing this simulation for a long time.

¹ The conclusion of this study is independent of the choice of the initial poloidal field.

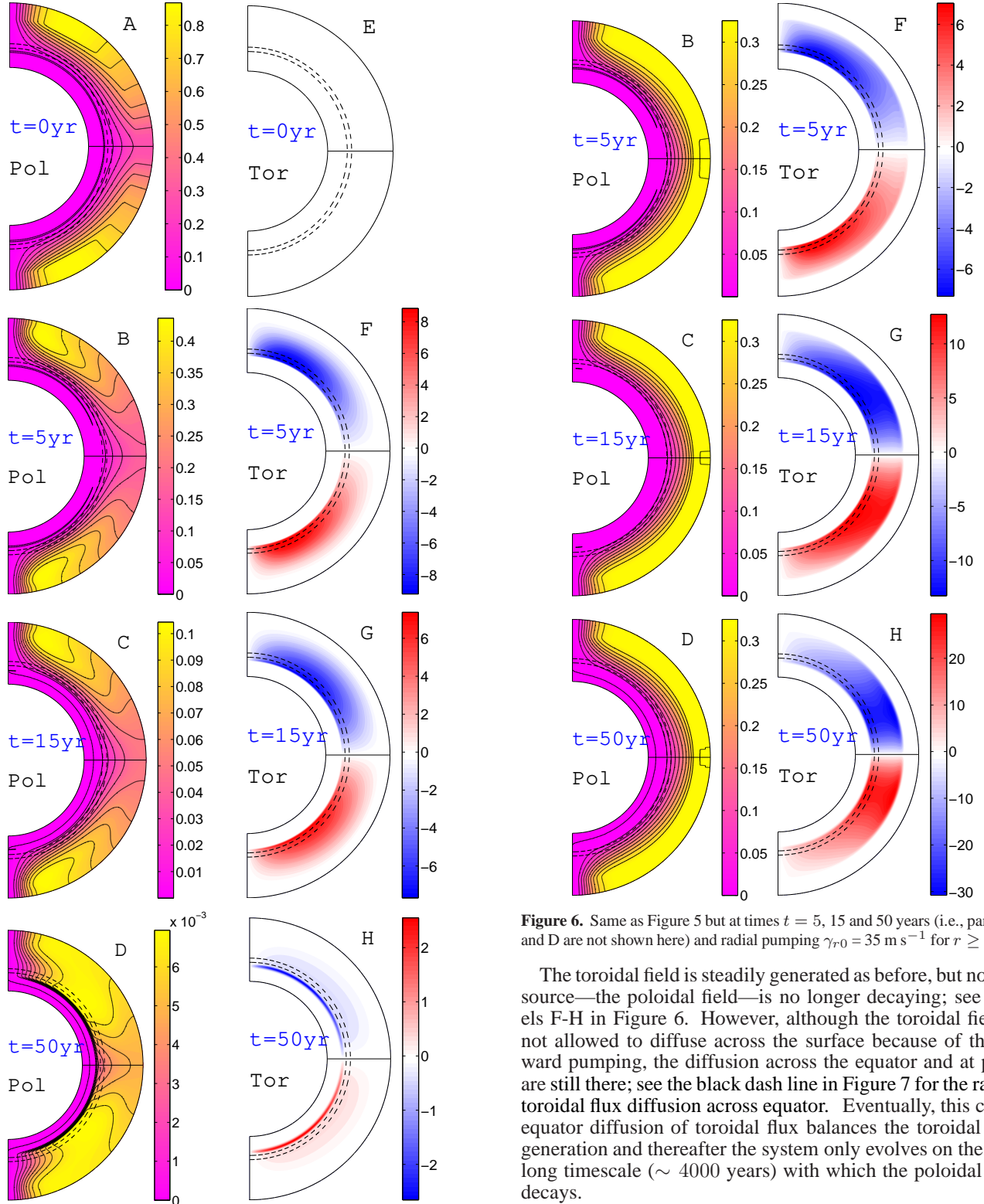


Figure 5. Snapshots of poloidal field defined by the contours of constant $r \sin \theta A$ (left panels) and the toroidal field (right) in r - θ planes at times $t = 0, 5, 15$ and 50 years. In this simulation $\eta_{CZ} = 5 \times 10^{11} \text{ cm}^2 \text{ s}^{-1}$, $\eta_{\text{surf}} = 3 \times 10^{12} \text{ cm}^2 \text{ s}^{-1}$, $\gamma_{r0} = 0 \text{ m s}^{-1}$ and $\alpha_0 = 0 \text{ m s}^{-1}$.

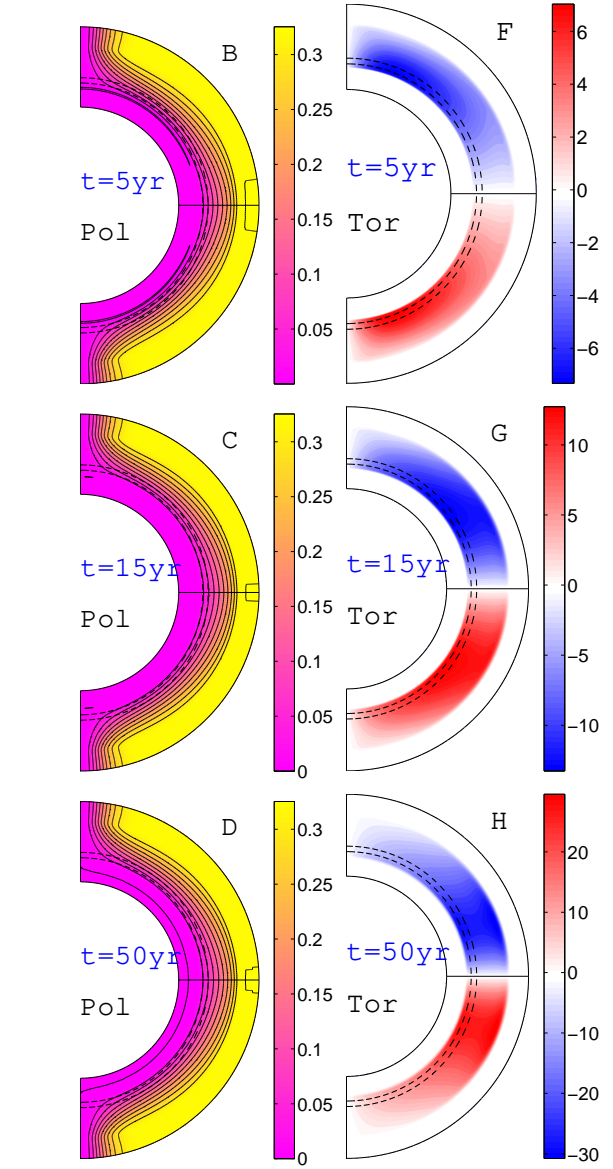


Figure 6. Same as Figure 5 but at times $t = 5, 15$ and 50 years (i.e., panels A and D are not shown here) and radial pumping $\gamma_{r0} = 35 \text{ m s}^{-1}$ for $r \geq 0.9R$.

The toroidal field is steadily generated as before, but now its source—the poloidal field—is no longer decaying; see panels F-H in Figure 6. However, although the toroidal field is not allowed to diffuse across the surface because of the inward pumping, the diffusion across the equator and at poles are still there; see the black dash line in Figure 7 for the rate of toroidal flux diffusion across equator. Eventually, this cross-equator diffusion of toroidal flux balances the toroidal field generation and thereafter the system only evolves on the very long timescale (~ 4000 years) with which the poloidal field decays.

3.2. Dynamo solutions with $\alpha^{\text{BL}} \neq 0$

Now we make $\alpha_0 \neq 0$ and perform a few sets of simulations by varying it within $[0.005-10] \text{ m s}^{-1}$. From now onward we consider the initial condition of our simulations as $B = \sin(2\theta) \sin[\pi(r - 0.7R)/(R - 0.7R)]$ for $r > 0.7R$ and 0 for $r \leq 0.7R$, while $A = 0$ for all r and θ . We run the simulation for several cycles so that our results are not much dependent

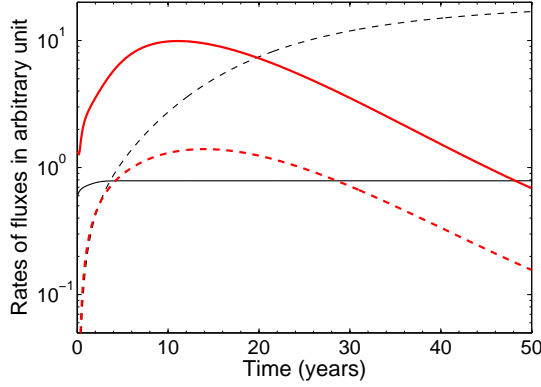


Figure 7. Rates of net diffusive toroidal fluxes across the solar surface (solid lines), and across the equator (dashed lines) for two simulations presented in Figures 5 and 6, without pumping (red/thick) and with 35 m/s pumping (black/thin), respectively.

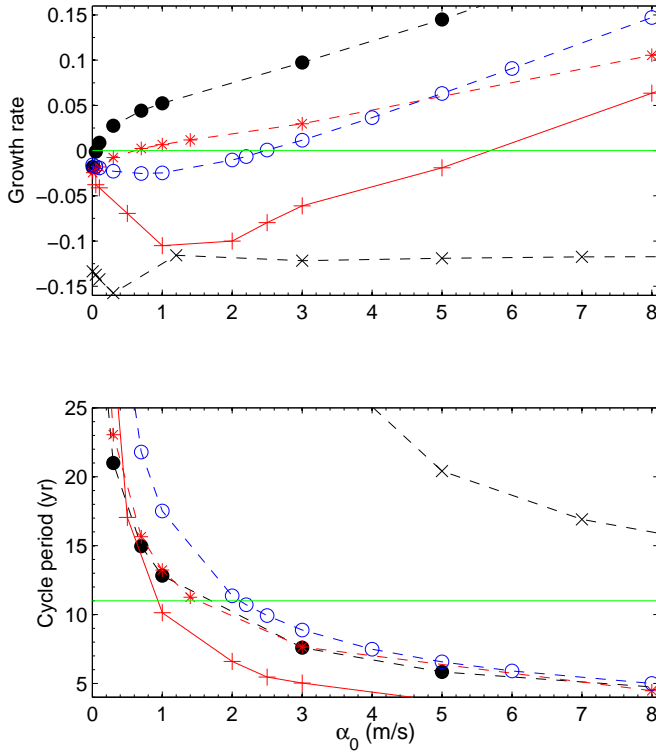


Figure 8. Results using the analytic rotation profile as shown in Figure 2: growth rates (per year) of the net toroidal flux in one hemisphere (upper panel) and the cycle period (lower panel) as functions of α_0 . Crosses represent simulations with $\eta_{CZ} = 5 \times 10^{11} \text{ cm}^2 \text{ s}^{-1}$ and no magnetic pumping ($\gamma_{r0} = 0$), while for all other symbols $\gamma_{r0} = 35 \text{ m s}^{-1}$. Filled points: $\eta_{CZ} = 5 \times 10^{11} \text{ cm}^2 \text{ s}^{-1}$, red asterisks: $\eta_{CZ} = 1 \times 10^{12} \text{ cm}^2 \text{ s}^{-1}$, open circles: same as filled points but with no equatorward component of meridional flow, and plus symbols: same as filled points but no meridional circulation.

on the initial condition.

When there is no magnetic pumping, the initial seed field decays like a damped oscillator for all values of α_0 in this range (expected based on the knowledge gained in previous decay experiments). Crosses in Figure 8 show the field decay rates (top) and the cycle periods (bottom). We notice that

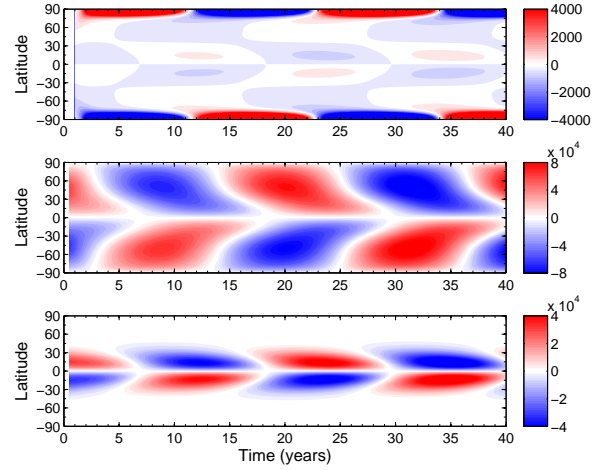


Figure 9. Time-latitude diagrams of the radial field (G) on the solar surface (top), mean toroidal field (G) over the whole CZ (middle) and the Babcock–Leighton source term, Equation (9) (bottom). In this simulation, $\alpha_0 = 1.4 \text{ m s}^{-1}$, $\eta_{\text{surf}} = 3 \times 10^{12} \text{ cm}^2 \text{ s}^{-1}$, $\eta_{CZ} = 1 \times 10^{12} \text{ cm}^2 \text{ s}^{-1}$ and $\gamma_{r0} = 35 \text{ m s}^{-1}$.

the cycle period decreases with increasing α_0 as expected in a linear $\alpha\Omega$ dynamo model. However, the dependence of period with α_0 in the FTD model is only mild (see Eq. (12) of Dikpati & Charbonneau 1999) possibly because of a strong B-dependent quenching introduced in the α effect.

Astonishingly, when the downward pumping of sufficient strength is present, results change completely. For α_0 below a certain value, the initial field still decays due to the diffusion, however above some critical value, we get growing oscillations. We note that in these simulations we have not considered any nonlinearity in Babcock–Leighton process to stabilize the dynamo growth. The filled circles in Figure 8 represent the results from simulations with 35 m s^{-1} downward pumping. Here we notice that the periods are much shorter compared to the simulations without pumping (as seen in the lower panel of the same figure). There are multiple reasons for producing such a short period. One is the longer lifetime (slower decay) of both the poloidal and toroidal fields due to the reduction in diffusion of flux through the photosphere as discussed above. Another is that the pumping helps to transport the field from the surface to the deeper layers of the CZ where the toroidal field can be amplified further and erupt to produce flux emergence (Karak & Nandy 2012).

For the parameters considered here, i.e., $\eta_{CZ} = 5 \times 10^{11} \text{ cm}^2 \text{ s}^{-1}$, $\eta_{\text{surf}} = 3 \times 10^{12} \text{ cm}^2 \text{ s}^{-1}$ and $\gamma_{r0} = 35 \text{ m s}^{-1}$, the dynamo period is nearly 63 years at near the critical value of α_0 for dynamo action (the growth rate for these parameters is 0.008 per year). Therefore, we perform a set of simulations at a higher value of diffusivity $\eta_{CZ} = 1 \times 10^{12} \text{ cm}^2 \text{ s}^{-1}$. Red asterisks in Figure 8 represent these. Here we get a nearly stable solution (growth rate = 0.01 per year) and 11-year period at $\alpha_0 = 1.4 \text{ m s}^{-1}$. Figure 9 shows the butterfly diagrams of the radial field, the mean toroidal field over the CZ and the Babcock–Leighton source term from this simulation. This figure displays most of the regular features of solar magnetic cycle e.g., the regular polarity reversal, correct phase relation between the radial and toroidal fields, the equatorward migration of toroidal field at low latitudes and the poleward migration of the surface radial field.

To understand the importance of the equatorward meridional flow we repeat the set of simulations at $\eta_{CZ} = 5 \times 10^{11} \text{ cm}^2 \text{ s}^{-1}$ and $\gamma_{r0} = 35 \text{ m s}^{-1}$ by making the equator-

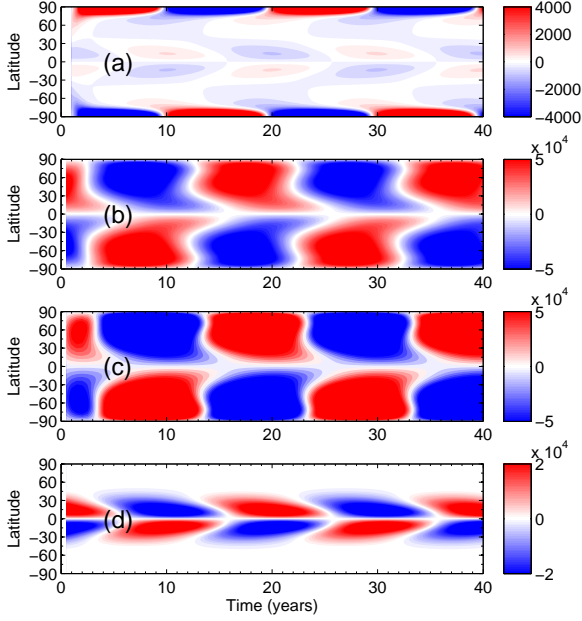


Figure 10. Same as Figure 9 except an additional panel (c), showing the toroidal field over tachocline and with different model parameters: $\alpha_0 = 2.5 \text{ m s}^{-1}$, $\eta_{CZ} = 5 \times 10^{11} \text{ cm}^2 \text{ s}^{-1}$ and *no equatorward component in the meridional flow*. (For better visibility of the weak fields, colorbars are clipped at displayed ranges.)

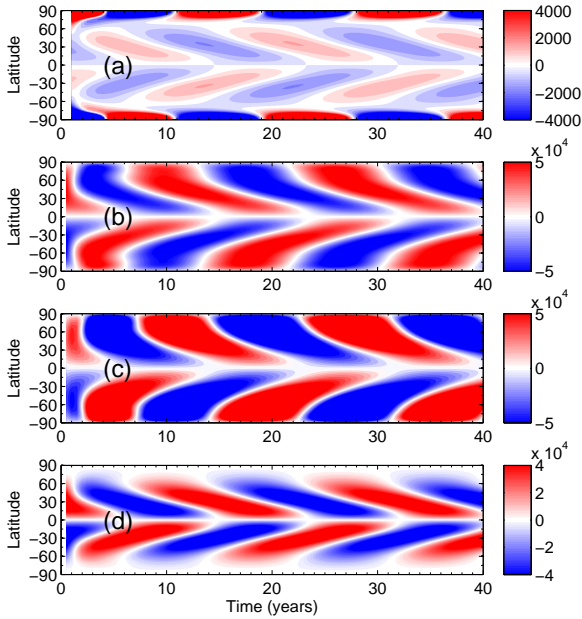


Figure 11. Same as Figure 10 but in this simulation $f_\alpha = \cos \theta \sin^2 \theta$ (i.e., $n = 2$ in Equation (11)) is used.

ward meridional flow (in the lower CZ) to zero. We emphasize that this setup is designed to disentangle the importance of equatorward meridional flow and the shear in the near-surface layer. However, we retain the poleward component of meridional flow in the upper CZ, which is crucial in producing the observed poleward migration of the radial field. To avoid

discontinuity, we do not change the radial component of the meridional flow and it remains as it is in the full meridional cell. This component is anyway very weak to affect the result. Instead of making this unphysical setup, we could, of course, consider a shallow meridional flow here. Nevertheless, this would contribute an equatorward flow at some depth and help to produce equatorward migration in toroidal field. Hence, to exclude the effect of the equatorward flow and to observe the consequence of the dynamo wave alone, we artificially cease the equatorward return flow. It is formally consistent with the kinematic mean-field equations where the mean meridional flow is prescribed. We comment that usually the meridional flow is assumed to satisfy $\nabla \cdot (\rho \mathbf{v}_p) = 0$ on the basis that the flow is steady and conserves mass, however in the mean-field framework mass conservation of a steady mean flow yields, $\nabla \cdot (\rho \mathbf{v}_p) = -\nabla \cdot (\overline{\rho' \mathbf{v}_p'})$, where primes indicate the fluctuating components and the overbar represents the resulting mean. The usual habit of using $\nabla \cdot (\rho \mathbf{v}_p) = 0$ reflects the fact that $-\nabla \cdot (\overline{\rho' \mathbf{v}_p'})$ is unprescribed by the model and treating it as anything other than zero introduces more parameters into a model that already has a large number of free parameters. For our purposes, setting the return flow to zero is not inconsistent in terms of the model.

The open circles in Figure 8 represent these simulations. Interestingly, we again find growing solutions for $\alpha_0 > 2.45 \text{ m s}^{-1}$. In Figure 10, we show the butterfly diagrams for $\alpha_0 = 2.5 \text{ m s}^{-1}$ (for which the growth rate = 0.0007 per year). The striking result is that we get a clear equatorward migration at low latitudes. As there is no equatorward meridional flow in these simulations, this equatorward migration is caused by the negative shear exists in the near-surface layer and the positive $\alpha^{\text{BL}}(r, \theta)$. This is a dynamo wave obeying the Parker–Yoshimura sign rule (Parker 1955; Yoshimura 1975). This result is in agreement with Guerrero & de Gouveia Dal Pino (2008) (see their Sec. 4) who found equatorward dynamo wave near the surface by including a NSSL. However, they need much weaker pumping ($< 1 \text{ m s}^{-1}$) than used here because the near-surface diffusivity is much smaller in Guerrero & de Gouveia Dal Pino (2008) than we use.

As our $\alpha^{\text{BL}}(r, \theta)$ is nonzero below $\approx \pm 30^\circ$ latitudes (where we see sunspots), we observe an equatorward migration only below $\approx \pm 30^\circ$ latitudes. Therefore when we extend the latitudinal width of $\alpha^{\text{BL}}(r, \theta)$ by changing f_α from $\cos \theta \sin^{12} \theta$ to $\cos \theta \sin^2 \theta$, we observe much prominent equatorward migration starting from higher latitudes than we found earlier; see Figure 11. This equatorward migration caused by the dynamo wave is not localized near the surface, rather it is propagated throughout the CZ; see Figure 10(c) and Figure 11(c). This is because the CZ is strongly radially coupled due to the high diffusivity as well as due to strong pumping operating in the upper part of the CZ.

Another feature to note is that the surface radial field (top panels of Figures 10 and 11) also propagates equatorward—as a consequence of dynamo wave—in low latitudes where $\alpha^{\text{BL}}(r, \theta)$ is nonzero, but shows a weak poleward migration in high latitudes—as a consequence of poleward meridional flow. Therefore, if the equatorward migration of butterfly wings of the Sun is really caused by the dynamo wave, then the α effect must be concentrated in low latitudes only (as we choose in our study by setting $f_\alpha = \cos \theta \sin^{12} \theta$), otherwise the poloidal field as a consequence of dynamo wave

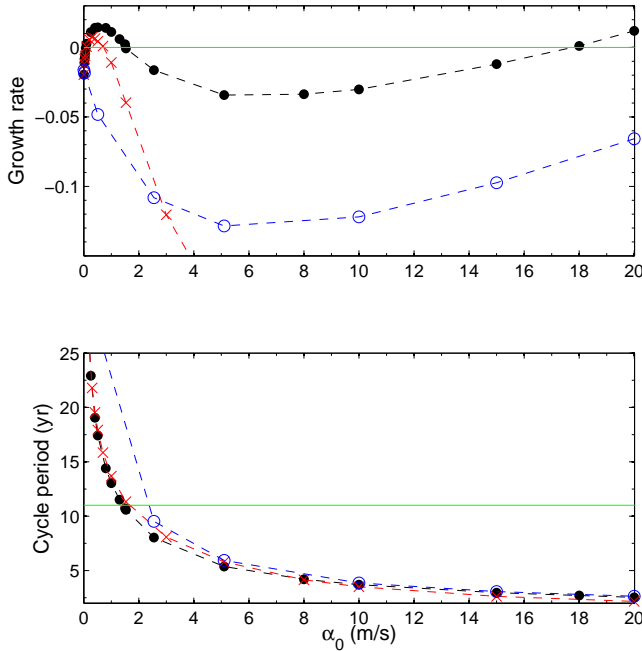


Figure 12. Results using the *observed* differential rotation as shown in Figure 3: Growth rates of toroidal flux (top) and the cycle periods (bottom) as functions of α_0 from simulations with $\gamma_{r0} = 35 \text{ m s}^{-1}$ and $\eta_{CZ} = 5 \times 10^{11} \text{ cm}^2 \text{ s}^{-1}$ (filled points). Red crosses represent simulations in which the radial shear in the near-surface shear is artificially set to zero, while open circles represent simulations with no equatorward meridional flow; everything else remain same in these two sets.

will migrate equatorward even in high latitudes which is not observed.

We further note that in these simulations, although the equatorward return flow was artificially switched off, its poleward component in the upper CZ was retained. This poleward meridional flow is crucial to transport the poloidal field generated through the Babcock–Leighton process at low latitudes. Therefore, if we switch off this surface-poleward flow, then the cycle period becomes shorter and the dynamo decays at these parameters. For details, we consider red plus symbols in Figure 8 which represent the set of simulations at $\eta_{\text{surf}} = 5 \times 10^{11} \text{ cm}^2 \text{ s}^{-1}$ and $\gamma_{r0} = 35 \text{ m s}^{-1}$ but no meridional flow. We observe that dynamo is growing only when $\alpha_0 \geq 6 \text{ m s}^{-1}$ but cycle periods are shorter. Thus in dynamo wave solution, although meridional flow is not required to produce the equatorward migration of Sun’s butterfly wings, the poleward surface flow is crucial to get a correct cycle period in the Sun.

4. DYNAMO SOLUTIONS WITH OBSERVED ROTATION PROFILE

We now perform simulations with the helioseismic data for angular velocity as shown in Figure 3(a). For the poloidal source, the α effect, we either relate it to the mean toroidal field in the CZ or in the tachocline.

4.1. Poloidal source relating to the mean toroidal field in CZ

Similar to previous studies we perform a few sets of simulations with $\eta_{CZ} = 5 \times 10^{11} \text{ cm}^2 \text{ s}^{-1}$ and $\gamma_{r0} = 35 \text{ m s}^{-1}$ by varying α_0 within $[0.003 - 20] \text{ m s}^{-1}$. The filled points in Figure 12 show the corresponding growth rates and dynamo periods. Here we see a non-monotonous behavior for growth

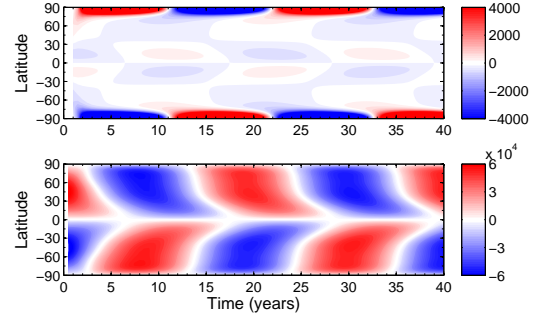


Figure 13. Results using the *observed* differential rotation, $\alpha_0 = 1.5 \text{ m s}^{-1}$, $\gamma_{r0} = 35 \text{ m s}^{-1}$ and $\eta_{CZ} = 5 \times 10^{11} \text{ cm}^2 \text{ s}^{-1}$. Time-latitude diagrams of the radial field on the solar surface (top) and the mean toroidal field over the whole CZ (bottom).

rate. For $0.1 \leq \alpha_0 \leq 1.5 \text{ m s}^{-1}$ we get positive growth, while for the intermediate value, $1.53 \leq \alpha_0 \leq 18 \text{ m s}^{-1}$, we have a region of unexpected negative growth. In Figure 13, we show the solution for $\alpha_0 = 1.5 \text{ m s}^{-1}$. Again this figure reproduces the basic features of the solar magnetic cycle.

Now we consider the other values of α_0 (filled circles) in Figure 12. With the increase of α_0 , the production of poloidal field is faster which makes the field reversal quicker, thereby making the cycle period shorter (as expected).

The decay for intermediate values of α_0 can be understood in the following way. In our model, the toroidal field is produced in the bulk of the CZ with the strongest production being at the high latitudes, while the poloidal field is produced from the toroidal field in low latitudes below 30° (where sunspot eruptions occur). At lower values of α_0 , the cycle period is long enough for the toroidal flux to be transported to the low latitudes to feed the flux emergence and subsequently the poloidal field generation. This transport of the toroidal flux is done by the equatorward flow because the advection time, say from latitude 60° to 15° is about 10 years for a 1 m s^{-1} meridional flow, while the diffusion time is about 100 years for $\eta_{CZ} = 5 \times 10^{11} \text{ cm}^2 \text{ s}^{-1}$. However at higher α_0 , when the cycle period becomes shorter than this advection time, the advection of toroidal field becomes less important. Hence the toroidal field at low latitudes decreases to make the production of the poloidal field weaker and consequently decay the oscillation. However, when α_0 is increased to a very large value, the cycle period does not decrease much (see Figure 12 bottom), but a stronger α_0 can produce a sufficient poloidal field even at a weaker toroidal field to make the dynamo growing again.

When we increase the diffusivity η_{CZ} above $7.5 \times 10^{11} \text{ cm}^2 \text{ s}^{-1}$, we get decaying solutions for all values of α_0 tested. We note that in the previous section, where we used the simplified profile for Ω , we had a growing dynamo solution with 11-year period even with a diffusivity of $10^{12} \text{ cm}^2 \text{ s}^{-1}$. This provides a measure of the sensitivity of dynamo action to the details of the differential rotation, pumping and diffusivity. We can definitely state that dynamo action is possible with turbulent magnetic diffusivities η_{CZ} up to about $7.5 \times 10^{11} \text{ cm}^2 \text{ s}^{-1}$, however there are enough free parameters and choices in the model to prevent us ruling out plausible solutions with higher diffusivities.

By repeating the set of simulations with $\eta_{CZ} = 5 \times 10^{11} \text{ cm}^2 \text{ s}^{-1}$ and $\gamma_{r0} = 35 \text{ m s}^{-1}$ with artificially zeroing the equatorward meridional flow near the bottom of CZ, we obtain decaying oscillations for all values of α_0 (open circles in Figure 12). The reason for this is already explained above.

When there is no flow near the bottom of the CZ, the toroidal field from high to low latitudes can only be reached by the diffusion (with diffusion time about 100 years). Therefore with the decrease of cycle period due to the increase of α_0 , the diffusion of the field from high to low latitudes decreases which effectively makes the production of the poloidal field weaker and causes the dynamo to decay. However it can again produce growing solutions at larger values of α_0 .

Finally, instead of putting the equatorward meridional flow to zero, we now repeat the above set of simulations by putting the radial shear in the near-surface layer to zero. The red crosses in Figure 12 represent this set. We obtain growing solutions for some smaller values of α_0 and then decaying at larger values. This behavior is very similar to the previous set of simulations with near-surface shear (filled points) except in this case the dynamo growth is smaller. Therefore the solutions with the observed differential rotation profile at smaller values of α_0 are FTD type, modified by the NSSL. At the highest values of α_0 we have considered, the dynamo-wave solution becomes more relevant, (although the solution without the equatorward return flow is still subcritical at this α_0).

4.2. Poloidal source relating to the tachocline toroidal field

In all previous simulations presented above, the Babcock–Leighton source, \overline{B} in Equation (9) was taken as the mean toroidal field over the whole CZ. Now we performed some simulations taking the Babcock–Leighton source \overline{B} to be the mean toroidal field in the tachocline. This is consistent with the prescription of the Babcock–Leighton process in the traditional FTD model (Dikpati & Charbonneau 1999; Karak et al. 2014a). Figure 14 displays the growth rates and the corresponding cycle periods as functions of α_0 from these simulations. When there is no magnetic pumping (crosses), the dynamo is always decaying unless α_0 is increased to a sufficiently larger value—consistent with the previous analysis. For $\gamma_{r0} = 35 \text{ m s}^{-1}$ and $\eta_{CZ} = 5 \times 10^{11} \text{ cm}^2 \text{ s}^{-1}$ (filled points), we observe growing solutions for any values of α_0 as long as it is above $\approx 0.02 \text{ m s}^{-1}$. For larger α_0 we get shorter period—consistent with previous simulations. However for $\eta_{CZ} = 7.5 \times 10^{11} \text{ cm}^2 \text{ s}^{-1}$ (squares) we get positive growth only for $\alpha_0 \geq 3 \text{ m s}^{-1}$ but the cycle period becomes somewhat short. Similar problem appears when either the equatorward component of meridional circulation is set to zero (open circles) or the full meridional circulation is set to zero (red pluses). For the case with no radial shear in the near-surface layer (triangles), we get growing oscillations for $\alpha_0 > 1 \text{ m s}^{-1}$ but cycle periods are again shorter than 11 years.

One may wonder how sensitive we are to the choice of 35 m s^{-1} for the magnetic pumping. To address this we take model with parameters: $\eta_{CZ} = 5 \times 10^{11} \text{ cm}^2 \text{ s}^{-1}$ and $\alpha_0 = 0.6 \text{ m s}^{-1}$ (represented by a filled point in Figure 14) and perform a set of simulations by varying the pumping speed γ_{r0} only. Growth rates and cycle periods from these simulations are displayed in Figure 15. We observe that the dynamo growth increases rapidly with the increase of pumping at lower values. This is expected because the downward pumping suppresses the diffusion of the field across the solar surface as explained in §3.1. Following Cameron et al. (2012), the dynamo growth rate becomes positive when the advection time by the pumping is at least five times the diffusion time. Thus by setting, $5d_{SL}/\gamma_{r0} = d_{SL}^2/\eta_{surf}$, (where

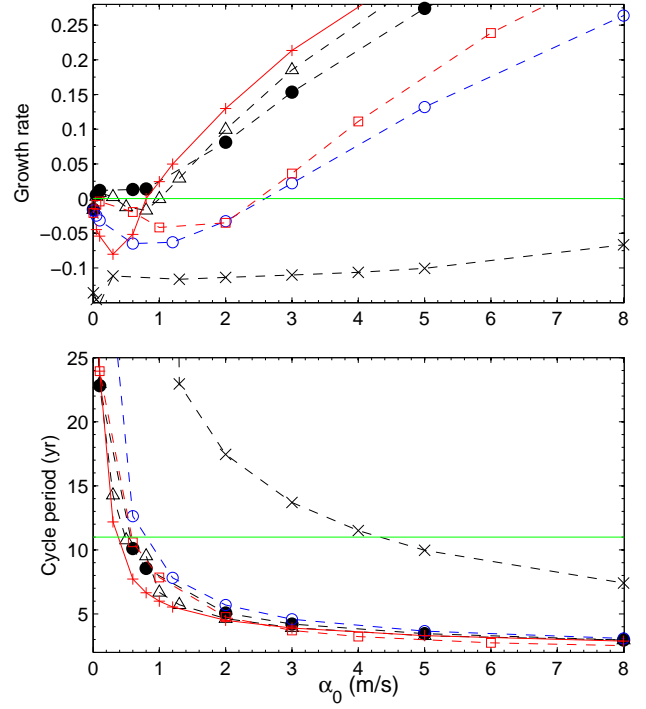


Figure 14. Growth rates of toroidal flux (top) and the cycle periods (bottom) as functions of α_0 from simulations in which the Babcock–Leighton source is related to the toroidal field in the tachocline. Crosses represent simulations with $\gamma_{r0} = 0$ and $\eta_{CZ} = 5 \times 10^{11} \text{ cm}^2 \text{ s}^{-1}$, while for all others $\gamma_{r0} = 35 \text{ m s}^{-1}$. For filled points and squares $\eta_{CZ} = 5 \times 10^{11} \text{ cm}^2 \text{ s}^{-1}$ and $7.5 \times 10^{11} \text{ cm}^2 \text{ s}^{-1}$, respectively. Open circles: same as filled points but the equatorward component of meridional flow is zero, triangles: same as filled points but no radial shear in the NSSL and red pluses: same as filled points except no meridional circulation.

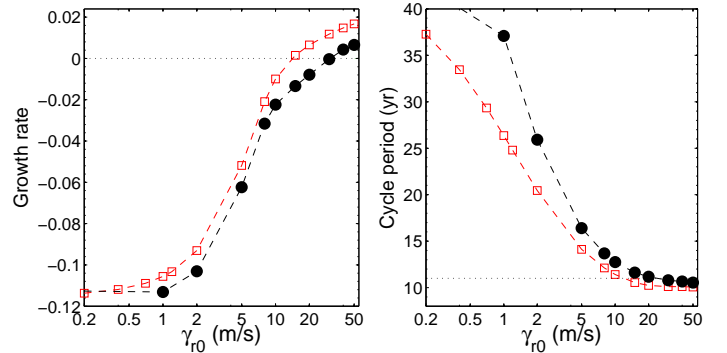


Figure 15. Growth rates (left panel) and cycle periods (right) as functions of pumping speed γ_{r0} (in log scale) for fixed values of other parameters. The black points correspond to simulations in which the Babcock–Leighton source is related to the mean toroidal field in the CZ and $\alpha_0 = 1.5 \text{ m s}^{-1}$, while for red squares, it is related to the tachocline toroidal field and $\alpha_0 = 0.6 \text{ m s}^{-1}$. For both sets $\eta_{CZ} = 5 \times 10^{11} \text{ cm}^2 \text{ s}^{-1}$ and $\eta_{surf} = 3 \times 10^{12} \text{ cm}^2 \text{ s}^{-1}$.

d_{SL} is the depth of the surface pumping layer $= 0.1R$) we obtain a rough estimate of the minimum γ_{r0} for the growing dynamo to be 20 m s^{-1} . This is indeed seen in Figure 15. However above this value, the pumping cannot help much and the dynamo growth will be limited by the cross-equator diffusion. For other set of simulations in which the Babcock–Leighton source is related to the mean toroidal field

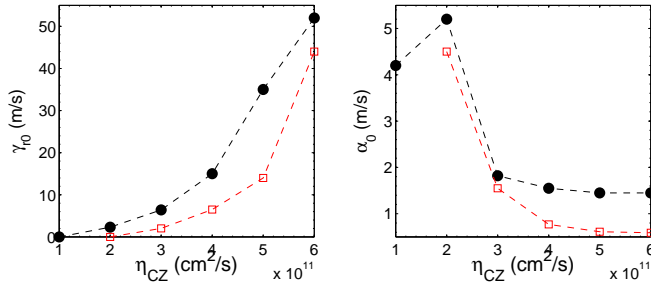


Figure 16. Left panel: downward pumping speed γ_{r0} needed to get 11-year cycle for different values of the bulk diffusivities η_{CZ} at a fixed value of the surface diffusivity η_{surf} of $3 \times 10^{12} \text{ cm}^2 \text{ s}^{-1}$. Black points and red squares represent two sets of simulations in which the Babcock–Leighton source is related to the mean toroidal field in the CZ and in the tachocline, respectively. Right panel: corresponding values of critical α_0 needed to get stable solutions.

in CZ (black points in Figure 15) we observe a similar trend although slightly smaller growth rates.

In the right panel of Figure 15, we observe a rapid decrease of cycle period with the increase of γ_{r0} at first and then saturation at larger values of γ_{r0} . The reduction of cycle period is due to the fact that pumping quickly transports the field from surface to the deeper CZ. For γ_{r0} in the range $[0.2\text{--}20] \text{ m s}^{-1}$, the cycle period $\propto \gamma_{r0}^{-0.3}$, which is a mild dependence compared to Eq. (5) of Guerrero & de Gouveia Dal Pino (2008) in the range $[0.2\text{--}1.2] \text{ m s}^{-1}$. The discrepancy is due to the fact that we are using pumping only near the surface and higher diffusivity.

Now we address the question, what is the minimum value of pumping required to get an 11-year solar cycle for a given value of diffusivity in the CZ. In Figure 16, we show this minimum pumping γ_{r0} for each value of η_{CZ} that can produce 11-year cycle period. We stress that in all these simulations η_{surf} and all other parameters, except α_0 remain unchanged. The α_0 is needed to vary because we make all the solutions critically/nearly stable (with dynamo growth rate essentially very small and positive)—thus for this set of simulations α_0 is not arbitrarily changed. Red squares in Figure 16 are obtained from simulations in which the Babcock–Leighton source is related to the tachocline toroidal field. We observe that when η_{CZ} is around $10^{11} \text{ cm}^2 \text{ s}^{-1}$ or less, we do not need any magnetic pumping to get an 11-year cycle. So at this point, our model essentially converges to the previous flux transport dynamo model. We recall that all previous flux transport dynamo models need around this much diffusivity to get an 11-year cycle period (e.g., Dikpati et al. 2002; Muñoz-Jaramillo et al. 2011; Jiang et al. 2013). The exact value of this critical diffusivity varies slightly from model to model as there are many other parameters that are not same in all previous models. However, from our study we show that as we increase the diffusivity, we need to increase the downward pumping. But when η_{CZ} is above around $6 \times 10^{11} \text{ cm}^2 \text{ s}^{-1}$, and the differential rotation is taken from helioseismic data, we fail to produce 11-year cycle even by increasing the pumping to an arbitrarily large value.

The black points in Figure 16 represent the results from simulations in which the Babcock–Leighton source is related to the mean toroidal field in the CZ. We observe that the results are essentially similar except that we need significantly larger pumping for the same parameters.

From the right panel of Figure 16, we note that the critical α_0 needed to get stable dynamo cycle decreases with the increase of η_{CZ} . This counterintuitive behavior is found be-

cause at higher η_{CZ} , higher pumping is needed and this higher pumping reduces the diffusion of the field to make the dynamo easier.

4.3. Solar cycle with a shallow meridional circulation

We have understood that the downward pumping enhances the equatorward migration produced in combination with the negative radial shear and the positive α^{BL} . A clear equatorward migration is still observed when there is no equatorward return flow in the deeper layer of CZ (Figures 10 and 11). This motivates us to perform a simulation with a shallow meridional circulation², for example residing only above $0.8R$ and no flow underneath. This scenario is very similar to the cases presented in Figure 1 of Hazra et al. (2014) and Figure 5 of Guerrero & de Gouveia Dal Pino (2008). The former authors showed that this type of a shallow meridional circulation is not able to produce an equatorward migration of the toroidal field rather it produces a poleward migration, while the latter authors showed that both an equatorward magnetic pumping and the dynamo wave due to the negative near-surface shear can produce an equatorward migration of the toroidal field, although the equatorward pumping alone produces the best result (see their Fig. 5). However when we perform the simulation with this type of meridional flow, we get a clear equatorward migration of toroidal field at low latitudes purely due to the negative near-surface shear as shown in Figure 17. Again this migration persists all the way to the tachocline as shown in Figure 17(e). This migration is now consistent with the observation.

The major difference between the present model and the Hazra et al. (2014) is that they did not include radial pumping, the near-surface shear and the radial magnetic boundary condition at the surface. On the other hand, Guerrero & de Gouveia Dal Pino (2008) used both radial and latitudinal pumpings as well as a negative shear at low latitudes. Both the latitudinal pumping and the negative shear were individually able to produce equatorward migration (see their Fig. 5-7). For our model to work we just need 9.8 m s^{-1} downward magnetic pumping in the upper layer of the Sun and a radial magnetic boundary condition at the surface. Our value of pumping is much higher than Guerrero & de Gouveia Dal Pino (2008) used because in our model, the turbulent diffusivity, particularly in the NSSL, is much higher.

In the present simulation, the Babcock–Leighton source is related to the toroidal field in the tachocline. However, we get a similar result with a clear equatorward migration when we perform the same simulation with the Babcock–Leighton source relating to the mean toroidal field in the CZ, except in this case we need $\gamma_{r0} = 11.5 \text{ m s}^{-1}$. This reveals that, although the amount of pumping needed in each model varies depending on the diffusivity and other parameters, the qualitative idea works. We recall that in earlier simulations, represented by open circles in Figures 12 and 14, when the equatorward component of the usual deep meridional circulation, was set to zero, produced decaying solutions. However here for a shallow meridional flow with no flow underneath $0.8R$, we get stable dynamo solution. The reason is that here we have an equatorward flow that helps to transport the toroidal

² To produce such a shallow meridional circulation, we used the following modified parameters: $\beta_1 = 3.5$, $\beta_2 = 3.3$, $\Gamma = 3.4 \text{ m}$, $R_p = 0.8R$, and the prefactor $r - R_p$ in Equation (5) is replaced by $1.0707(r - R_p)^{0.3}[1 - \text{erf}\{(r - 0.87R)/1.5\}]$.

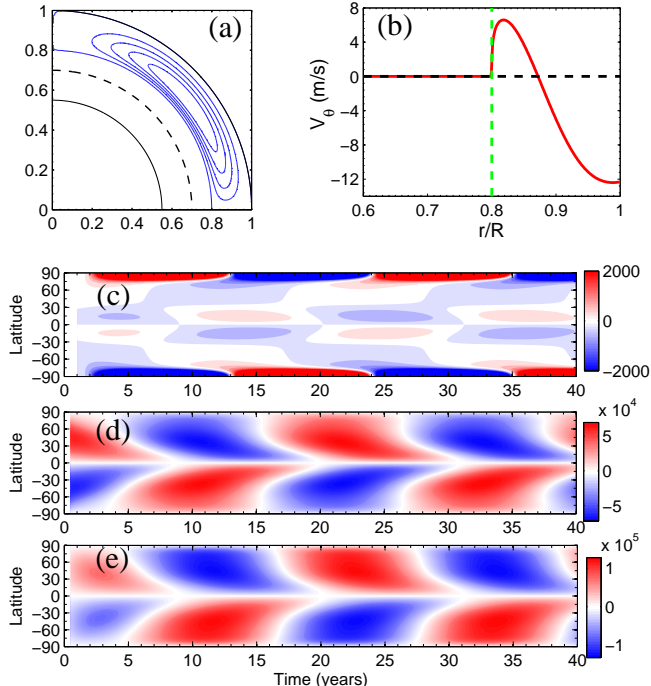


Figure 17. (a) Streamlines of a shallow meridional circulation with no flow below shown for the northern hemisphere only. (b) Radial variation of v_θ at 45° latitude. Butterfly diagrams of: (c) surface radial field, (d) the mean toroidal field in the CZ and (e) the toroidal field in the tachocline. In this simulation $\eta_{CZ} = 5 \times 10^{11} \text{ cm}^2 \text{ s}^{-1}$ and $\gamma_{r0} = 9.8 \text{ m s}^{-1}$.

field from high to low latitudes where the α^{BL} works.

5. CONCLUSION AND DISCUSSION

We have revisited two fundamental features of the sunspot cycle: the equatorward migration and the 11-year periodicity, using a dynamo model in which the poloidal field is generated through the Babcock–Leighton process near the solar surface at low latitudes, whereas the toroidal field is generated through the stretching of poloidal field by differential rotation which is constrained by the helioseismology. Our model also includes a single-cell meridional flow of which the surface flow is consistent with observations. The poleward flow near the surface is crucial for advecting the poloidal field towards the pole and thereby producing the observed poleward migration of the radial field on the surface. The poleward flow is also crucial to store the poloidal field in high latitudes for a sufficiently long time. Whereas the equatorward component of the meridional flow gives the equatorward migration of toroidal field near the bottom of CZ, consistent with previous flux transport dynamo models (Choudhuri et al. 1995; Durney 1995). However, we show that equatorward meridional flow is not the only solution for this. We show that when we have a reasonable amount of magnetic pumping in the upper layer of the Sun, the equatorward migration of the toroidal field is observed at low latitudes as a consequence of the dynamo wave (following Parker–Yoshimura sign rule with positive α^{BL} in the northern hemisphere and negative shear) even when there is no equatorward flow near the bottom of the CZ, although the cycle period becomes short (6 years rather than 11 years) when we use the helioseismic differential rotation profile. By reducing the surface diffusion, η_{surf} and α_0 , we can achieve an 11-year period in this case too, but the dynamo tends to produce a quadrupolar field which is not

solar-like (see Chatterjee et al. 2004, who demonstrated that a strong surface diffusion is crucial to get dipolar fields). We note that if the surface poleward flow is also switched off in the dynamo wave case, then the cycle period becomes short again and the dynamo becomes weaker (consistent with the ideas of Roberts & Stix 1972).

In the case where we use the fully observed differential rotation we get a FTD type solution modified by the NSSL consistent with Guerrero & de Gouveia Dal Pino (2008) and the distributed model of Käpylä et al. (2006). Because both terms play a role, we get a clear equatorward migration with a shallow meridional flow residing above $0.8R$ (Figure 17). The main difference between dynamo wave and FTD solutions is in the value of α_0 required to get growing solutions with the correct period.

In all these simulations, the magnetic pumping plays a crucial role in suppressing the diffusion of fields across the surface. This helps us to achieve dynamo at a significantly higher value of diffusivity in the bulk. For pumping $\gamma_{r0} = 35 \text{ m s}^{-1}$ and surface diffusivity $\eta_{\text{surf}} = 3 \times 10^{12} \text{ cm}^2 \text{ s}^{-1}$, we find a dynamo solution with an 11-year period at a bulk diffusivity $\eta_{CZ} = 5 \times 10^{11} \text{ cm}^2 \text{ s}^{-1}$, which is 5 times larger than the allowed value when there is no magnetic pumping (see Figure 16 for details). However, if the Babcock–Leighton source is related to the toroidal field near the bottom of the CZ, which is the usual prescription in flux transport dynamo models, then our model works even at smaller magnetic pumping (about 10 m s^{-1} for above parameters).

For $\eta_{CZ} > 5 \times 10^{11} \text{ cm}^2 \text{ s}^{-1}$, in the part of parameter space we have sampled, we do not get an 11-year cycle. We could obtain dynamo solutions with the correct period and equatorial propagation at a diffusivity of $10^{12} \text{ cm}^2 \text{ s}^{-1}$ using a simplified version of the differential rotation, which gives an indication of our sensitivity to the differential rotation, pumping and choice of diffusivity profile. While this is still an order of magnitude less than expected from mixing length arguments, it is close to the values suggested from the study of Cameron & Schüssler (2016). All previous flux transport dynamo models were constructed with a diffusivity much weaker than $10^{12} \text{ cm}^2 \text{ s}^{-1}$ (Muñoz-Jaramillo et al. 2011; Miesch & Teweldebirhan 2016). Although Choudhuri and his colleagues (Chatterjee et al. 2004, and the publications later) have used the diffusivity for poloidal field $\approx 10^{12} \text{ cm}^2 \text{ s}^{-1}$, the diffusivity for toroidal field is reduced by a factor of about 60. On the other hand, Kitchatinov & Olemskoy (2012) have used a diffusivity $\sim 10^{13} \text{ cm}^2 \text{ s}^{-1}$ in the bulk of CZ, consistent with the mixing-length value, but they reduce it by four orders of magnitudes below $0.75R$ and a diamagnetic pumping is considered there. In this article, we have shown that a moderately high value of the diffusivity (5×10^{11} to $10^{12} \text{ cm}^2 \text{ s}^{-1}$) is plausible given a sufficiently strong pumping near the surface. Such pumping is possible near the solar surface and has been shown to be necessary in order to make the FTD model compatible with surface observations (Cameron et al. 2012).

We thank Mark Miesch, Jie Jiang and the anonymous referee for careful review this article and providing valuable comments which improved the clarity of the presentation. BBK is supported by the NASA Living With a Star Jack Eddy Postdoctoral Fellowship Program, administered by the University Corporation for Atmospheric Research. The National Center for Atmospheric Research is sponsored by the

National Science Foundation.

REFERENCES

- Augustson, K., Brun, A. S., Miesch, M., & Toomre, J. 2015, *ApJ*, 809, 149
- Brandenburg, A. 2005, *ApJ*, 625, 539
- Brandenburg, A. 2009, in *IAU Symposium*, Vol. 259, IAU Symposium, ed. K. G. Strassmeier, A. G. Kosovichev, & J. E. Beckman, 159–166
- Brandenburg, A., Tuominen, I., Nordlund, A., Pulkkinen, P., & Stein, R. F. 1990, *A&A*, 232, 277
- Brown, B. P., Browning, M. K., Brun, A. S., Miesch, M. S., & Toomre, J. 2010, *ApJ*, 711, 424
- Cameron, R., & Schüssler, M. 2015, *Science*, 347, 1333
- Cameron, R. H., Schmitt, D., Jiang, J., & Işık, E. 2012, *A&A*, 542, A127
- Cameron, R. H., & Schüssler, M. 2016, *A&A*, 591, A46
- Charbonneau, P. 2014, *Ann. Rev. Astron. Astrophys.*, 52, 251
- Chatterjee, P., Nandy, D., & Choudhuri, A. R. 2004, *A&A*, 427, 1019
- Choudhuri, A. R., Schüssler, M., & Dikpati, M. 1995, *A&A*, 303, L29
- Dasi-Espuig, M., Solanki, S. K., Krivova, N. A., Cameron, R., & Peñuela, T. 2010, *A&A*, 518, A7
- Dikpati, M., & Charbonneau, P. 1999, *ApJ*, 518, 508
- Dikpati, M., Corbard, T., Thompson, M. J., & Gilman, P. A. 2002, *ApJ*, 575, L41
- Drobyshevski, E. M., & Yuferev, V. S. 1974, *Journal of Fluid Mechanics*, 65, 33
- Durney, B. R. 1995, *Sol. Phys.*, 160, 213
- Guerrero, G., & de Gouveia Dal Pino, E. M. 2008, *A&A*, 485, 267
- Guerrero, G., Dikpati, M., & de Gouveia Dal Pino, E. M. 2009, *ApJ*, 701, 725
- Hanasoge, S. M., Duvall, T. L., & Sreenivasan, K. R. 2012, *Proceedings of the National Academy of Science*, 109, 11928
- Hazra, G., Karak, B. B., & Choudhuri, A. R. 2014, *ApJ*, 782, 93
- Jiang, J., Cameron, R. H., Schmitt, D., & Işık, E. 2013, *A&A*, 553, A128
- Käpylä, P. J., & Brandenburg, A. 2009, *ApJ*, 699, 1059
- Käpylä, P. J., Korpi, M. J., & Brandenburg, A. 2009, *A&A*, 500, 633
- Käpylä, P. J., Korpi, M. J., & Tuominen, I. 2006, *Astronomische Nachrichten*, 327, 884
- Karak, B. B. 2010, *ApJ*, 724, 1021
- Karak, B. B., & Choudhuri, A. R. 2012, *Sol. Phys.*, 278, 137
- Karak, B. B., Jiang, J., Miesch, M. S., Charbonneau, P., & Choudhuri, A. R. 2014a, *Space Sci. Rev.*, 186, 561
- Karak, B. B., Kitchatinov, L. L., & Choudhuri, A. R. 2014b, *ApJ*, 791, 59
- Karak, B. B., & Nandy, D. 2012, *ApJ*, 761, L13
- Karak, B. B., Rheinhardt, M., Brandenburg, A., Käpylä, P. J., & Käpylä, M. J. 2014c, *ApJ*, 795, 16
- Kitchatinov, L. L., & Olemskoy, S. V. 2011, *Astronomy Letters*, 37, 656
- . 2012, *Sol. Phys.*, 276, 3
- Köhler, H. 1973, *A&A*, 25, 467
- Komm, R. W., Howard, R. F., & Harvey, J. W. 1995, *Sol. Phys.*, 158, 213
- Krause, F., & Rädler, K. H. 1980, *Mean-field magnetohydrodynamics and dynamo theory* (Oxford: Pergamon Press)
- Lemerle, A., Charbonneau, P., & Carignan-Dugas, A. 2015, *ApJ*, 810, 78
- Miesch, M. S., & Teweldeberhan, K. 2016, *Space Sci. Rev.*
- Muñoz-Jaramillo, A., Nandy, D., & Martens, P. C. H. 2011, *ApJ*, 727, L23
- Parker, E. N. 1955, *ApJ*, 122, 293
- . 1975, *ApJ*, 198, 205
- Petrovay, K., & Szakaly, G. 1993, *A&A*, 274, 543
- Pipin, V. V., & Kosovichev, A. G. 2011, *ApJ*, 727, L45
- Roberts, P. H., & Stix, M. 1972, *A&A*, 18, 453
- Rüdiger, G., Kitchatinov, L. L., Küker, M., & Schultz, M. 1994, *Geophysical and Astrophysical Fluid Dynamics*, 78, 247
- Simard, C., Charbonneau, P., & Dube, C. 2016, *ArXiv e-prints*
- Spruit, H. 1997, *Mem. Soc. Astron. Italiana*, 68, 397
- Spruit, H. C. 2011, in *The Sun, the Solar Wind, and the Heliosphere*, ed. M. P. Miralles & J. Sánchez Almeida, pp39
- Tobias, S. M., Brummell, N. H., Clune, T. L., & Toomre, J. 1998, *ApJ*, 502, L177
- Vasil, G. M., & Brummell, N. H. 2009, *ApJ*, 690, 783
- Wang, Y.-M., Sheeley, Jr., N. R., & Nash, A. G. 1991, *ApJ*, 383, 431
- Warnecke, J., Rheinhardt, M., Käpylä, P. J., Käpylä, M. J., & Brandenburg, A. 2016, *ApJ*
- Weber, M. A., & Fan, Y. 2015, *Sol. Phys.*, 290, 1295
- Yoshimura, H. 1975, *ApJ*, 201, 740